Shaping of geopolymer composites by 3D printing

Julien Archez, Nathalie Texier-Mandoki, Xavier Bourbon, Jean-François F Caron, Sylvie Rossignol

Shaping of geopolymer composites by 3D printing

J. Archez[1,2,3], N. Texier-Mandoki[2], X. Bourbon[2], J.F. Caron[3] and S. Rossignol[1]

[1] IRCER: Institut de Recherche sur les Céramiques (UMR7315), 12 rue Atlantis, 87068 Limoges Cedex, France.

[2] Agence nationale pour la gestion des déchets radioactifs (Andra), 1/7 rue Jean-Monnet 92298 Chatenay-Malabry Cedex, France.

[3] Laboratoire Navier, UMR 8205, Ecole des Ponts, CNRS, UPE, Champs-sur-Marne, France

■ Corresponding author: sylvie.rossignol@unilim.fr, tel.: 33 5 87 50 25 64

Abstract

This work aims to shape a hollow cylinder with a geopolymer and an additive manufacturing process (3D printing) without organic additives. The formulation of a geopolymer composite using only mineral parts is proposed and the parameters of the 3D printing process were optimized. The mechanical properties, the microstructure, and the adhesion of the layers of the printing material were analysed and compared with the literature. The results showed that the geopolymer composite could be printed with the addition of small ratios of wollastonite, glass fibers, or non-reactive aluminosilicate and by modifying the printing speed. The stacking layers exhibited a good adhesion between them, avoiding the so-called "cold joints" effect, and the fibers are flow-oriented during the process. Some hollow cylinders are successfully printed with a flexural strength of 15 MPa.

Keywords: Geopolymer, Composite, Additive manufacturing, Slump, Microstructure, Flexural Strength.

Highlights:

- Geopolymer composites were shaped by additive manufacturing (robocasting).
- The slump rate was reduced with the optimisation of the formulation.
- The layers exhibit a good adhesion and the fibers are oriented.
- A flexural strength of 15 MPa was obtained for the printed material.
- The mechanical properties are a bit higher than the values found in the literature.

Graphical abstract:

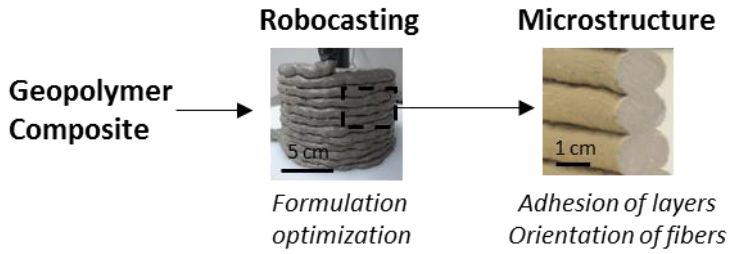

1. INTRODUCTION

Cigéo is the radioactive waste disposal facility project led by the French National Radioactive Waste Management Agency (Andra) for long-term management of the high and intermediate-level radioactive waste. The high-level radioactive waste cell concept is based on a steel liner inserted in a small tunnel dug in a sedimentary geological medium. Its primary function is mechanical to ensure safety, security, and retrievability during the operating phase. The use of geopolymers reinforced with inorganic elements could be an innovative solution for the liner to reduce metallic use in the project. To meet the mechanical specifications of the liner, geopolymer composites are considered.

Geopolymers are inorganic materials that present physical and chemical properties interesting for candidate materials in various applications but with an identified weakness: their mechanical properties, especially their tensile and flexural strength [i]. Alkali-activated materials, made with co-product, fly ash or slag lead to the formation of alumino-silicate hydrate and present different reaction mechanisms and properties than geopolymers [ii, iii, iv]. They are therefore distinguished, here, from the metakaolin-based geopolymers. The addition of fibers in geopolymers leads to an improvement of the ductility of the material by monitoring the crack opening and its diffusion throughout the material [v, vi]. It also permits to obtain satisfactory mechanical strength up to 110 MPa in compression and 17 MPa in flexion [vii]. Glass fibers [viii] and wollastonite [ix] have already been used in the literature. The influence of these reinforcements to form a geopolymer composite and improve the mechanical properties have also been studied previously for this project [x]. Freshly prepared geopolymers are liquid with various viscosity and, as ceramic solution or suspension, they are usually shaped by casting [xi, xii]. However, the addition of wollastonite [xiii] or glass fibers [xiv], increases the viscosity and decreases the workability (castability) of the material.

This paper aims to propose and test a process that permits the shaping of a geopolymer with an improved mechanical strength. Additive manufacturing or 3D printing process (automated extrusion of a lace and stacking deposition in three dimensions of space) [xv] is naturally an interesting alternative to the traditional casting. Avoiding mould, this process represents undoubtedly a real innovation. Classical for plastics and polymers, it is also widely developed during the last decade for concrete in the building industry [xvi]. The 3D printing process has also been used with geopolymers by Franchin et al. [xvii] at a small scale (nozzle size from 100 to 1500 µm) with the utilization of organic additives (poly(acrylic acid) *PAA* or poly(ethylenglycol) *PEG*) to adapt the rheology of the geopolymer to the process. At a larger scale, micro-algal has also been used to print geopolymer material with a structure of 45 cm [xviii]. In cement and concrete materials, additives like water reducers [xix], ticker agents, or superplasticizers [xx] are commonly used to control the rheology of the printed material [xxi]. Hydration inhibitor, retarder agent, or setting accelerator [xxii] are also added to control the setting time. In the case of alkali-activated materials, the rheology of printed materials is controlled by the content of fly ash, slags, or silica fume [xxiii]. It has been shown that the addition of nanoclay in the alkali-activated materials increases the thixotropy and the printing due to the flocculation of the clay particles [xxiv]. Moreover, the addition of hydromagnesite seeds can increase the rate of the hydration reaction and early strength development improving the buildability of the alkali-activated material [xxv]. The use of organic additives [xxvi] plasticizer [xxvii] or gelling agent [xxviii] is also often use to print the material. However, the European regulation, namely the Registration, Evaluation, Authorization, and Restriction of Chemicals (REACH) calls for the progressive substitution of the most dangerous chemicals when suitable alternatives have been identified and to limit the use of volatile organic compounds [xxix].

The first important aspect to check is the strength of the inter-layer bond and the mechanical strength of the material printed. In the literature, several printed specimens are usually tested in compression and bending, highlighting mechanical anisotropic behaviors regarding the orientation of the mechanical constraint. As mentioned by Buswell et al. [xvi], it is important to note that there are no standards adapted for the samples made by additive manufacturing. Every author uses different manufacturing parameters (nozzle diameter, printing speed, layer height) or different specimens (dimensions, number of layers). The comparison of the results has then to be taken with caution. Nematollahi et al. [xxx] and Panda et al. [xxxi] showed that the superposition of layers of alkali-activated materials leads to an anisotropic material as the fresh material is free to settle and expand in one direction but is compacted in the other direction due to the self-weight of the material. This anisotropic behaviour has also been underlined for concrete and alkali-activated materials with the presence of fibers due to their orientation during extrusion which tends to improve the flexural resistance perpendicularly of the orientation of fibers [xxxi, xxxii]. Moreover, some authors [xxxiii, xxxiv, xxxv] showed that a high time interval between concrete layers creates “cold joint” due to an excessive drying at the surface of the lace: if the surface is too dry and/or if the material has started to set, it does not create a strong bond with the fresh material. Panda et al. [xxxvi] and Al-Qutaifi et al. [xxxvii] studied the inter-layer bond strength of an alkali-activated material and shown that the interlayer bond strength decreases when the time interval, the speed of the nozzle but also the nozzle distance increases. The stiffness of the extruded material can also lead to the appearance of voids. A non-adapted shape [xxxviii, xxxix] or the addition of fibers [xl, xli] can also create voids between the extruded filaments leading to a decrease in the inter-layer bond strength. The 3D printing parameters and the formulation play thus an important role in the adhesion of layers and the mechanical properties of the printed material. As the printing is always studied in the literature with alkali-activated materials or with the use of organic additives, it needs to be

studied with the developed organic free composition of composite geopolymer. Consequently, this work aims to propose new solutions using inorganic additives, like the wollastonite or glass fibers, to form a printable composite. Different formulations and ratios were then tested, printings were realized and the properties of the printed sample were analyzed.

2. EXPERIMENTS

In this part, after a presentation of the raw material compositions and the fabrication process, the characterization methodology is described, including microscopic observation, and mechanical tests.

2.1 Raw material and samples preparation

The geopolymer composites are obtained by dissolving an aluminosilicate source in a potassium silicate solution followed by the addition of reinforcement elements and pulverised powders mixed ten minutes until homogenization [x]. The raw materials data are presented in **Table 1**. The potassium silicate solution is provided by Woellner and has a potassium concentration of 7 mol/L. The aluminosilicate sources are two metakaolins (M1 and M2) chosen regarding their chemical reactivity discrepancies [xlii] and Callovo-Oxfordian argillites (A650), comes from the underground laboratory of Andra and has been calcined at 650 °C with a static furnace to enhance its chemical reactivity [xliii]. Those aluminosilicate sources present different reactivity and therefore different setting time and reaction kinetic [xliii, xliv]. Reinforcements elements are acicular needles of wollastonite (W) and alkali-resistant glass fibers (G). Powdered fillers are non-reactive aluminosilicate sources (kaolin (Ki) or raw Callovo-Oxfordian argillites (A) and sand (Sa).

The nomenclature used is $M_xW_aG_bA_cKi_dSa_e$, where *x* refers to the quantity of metakaolin M1 in grams, added in 15,6 g of alkaline solution. One formulation was used with different aluminosilicate source (12 g of M1, 1.4 g of M2 and 3.2 g of A650) and is mentioned as M*. "*a, b, c, d,* and *e"* represent the weight percentage relative to the mass of the binder (S3 + M1)

of wollastonite, glass fibers, raw argillite, kaolin, and sand respectively. As an example, for 15,6 g of solution, 16 g of metakaolin M1, 6.64 g of wollastonite W and 0.63 g of glass fibers G and 1.90g of sand Sa, the composite will be referenced as $M_{16}W_{21}G_2Sa_6$. The formulations used are listed in **Table 2**.

2.2 Shaping processes

Casting and additive manufacturing processes are used to shape the geopolymer composite. Flexural specimens are cast in silicon prismatic molds (20 x 20 x 100 mm) and placed on a vibrating table (50 Hz) for five minutes to limit the air bubbles. Specimens are also printed (Φ_{nozzle} = 10 mm) with 2 layers wide and 3 layers high to be tested in bending test in a lateral and perpendicular direction compared to the printing orientation, as shown in **Figure 1**. All the samples are rectified to obtain plane surfaces and a dimension of 20 x 20 x 100 mm. Samples are stored at 20°C and 85 % HR and tested after 7 days. For the additive manufacturing process, the reactive mixture is deposited layer by layer using a 3D printer Potterbot 7© (**Figure 2–a**). The printing path (gcode) is designed with Rhinoceros/Grasshopper software. The flow is set manually during the printing to keep a constant layer width. During printing, the height between two layers (h), the nozzle speed (v_n), and the printing path (P) are maintained identical (**Figure 2-b**). To keep a printing speed constant, the nozzle speed is calculated depending on the printing path. The layer height (h) is equal to 66 % of the nozzle diameter to enhance the layer adhesion. The printing speed is indeed equal to the speed of the nozzle (v_n in m/s) multiply by the layer height (h in m) and divided by the printing path (P in m) **(1)**. The printing speed should be low enough to prevent the layers to slump under their weight and fast enough for the layers to adhere to each other. For instance, to obtain a printing speed of 62.10^{-6} m/s, the nozzle speed, the layer height and, the printing path were equal to 3.10^{-3} m/s, $6.5.10^{-3}$ m and 0.314 m respectively.

$$v_z = \frac{v_n \times h}{P} \quad \textbf{(1)}$$

To quantify the behavior of the samples, the slump rate (A in %) is calculated by measuring the height of several layers (hm) compared by the height of the layers issued from the gcode h_g **(2)**, (**Figure 2-b**). The more the slump was low, the more the printing quality was high as the nozzle distance remained low.

$$\mathbf{A}\ (\%) = \frac{h_g - \mathbf{h_m}}{h_g} \qquad \mathbf{(2)}$$

2.3 Sample characterization

The consolidation of the reactive mixture is followed over time with an environmental scanning electron microscope (ESEM) Quanta FEG 450. After mixing, the reactive mixture is extruded manually with a syringe (Φ = 2 mm) on copper support (Φ = 10 mm) and the sample is immediately placed in the ESEM and observed until consolidation. A void of 1000 Pa was maintained with a Peltier module with different conditions of humidity and temperature (43 % RH / 20 °C, 63 % RH / 14 °C and 93 % RH, 8°C). The morphology of the final material is observed using a JEOL IT 300 LV scanning electron microscope at 10 kV. A 10 nm layer of Pt is deposited on samples before observations.

The three-point bending test is carried out with an Instron 6022 apparatus, a span of 60 mm, a constant speed of 5 µm.s^{1}, and a load cell of 10 kN. The strain is measured with a strain gauge (Model KFGS-5-120-C1-11, Kyowa Electronic Instruments) centered under the sample, where the strain is maximum. The Young's modulus is determined by measuring the slope at the origin of the stress/strain curve.

3. RESULTS AND DISCUSSION

In this part, the influence of the geopolymer composite formulation and the printing speed are first investigated to reduce the slump observed during the printing. The adhesion of layers is then investigated by microstructure analysis. The mechanical properties of samples made by casting and 3D printing are finally analysed and compared to the literature data.

3.1 Influence of the formulation adjustment on the slump at a constant printing speed

The formulation of geopolymer composite and the influence of wollastonite and glass fibers on the viscosity of the reactive mixture and the working properties of the consolidated materials has been previously studied [x, xlv]. Consequently, three formulations were first selected, with different amount of wollastonite ($M_{16}W_2G_2$, $M_{16}W_{10}G_2$) and with the addition of raw argillite ($M_{16}W_{10}G_2A_{10}$), in order to evaluate the feasibility of shaping by additive manufacturing. Hollow cylinder (Φ = 10 cm) were elaborated with these formulations and a constant vertical printing speed (= 62.10^{-6} m/s). The slump rate and the corresponding photos are gathered in **Table 3.** The composition $M_{16}W_2G_2$ presents a slump rate of 67 % that does not allow enough layers to be stacked to obtain a cylinder. After several layers, the height of the nozzle is indeed too high and the material doesn't follow the printing speed anymore. An addition of wollastonite ($M_{16}W_{10}G_2$) and argillite ($M_{16}W_{10}G_2A_{10}$) allows decreasing of the slump rate from 32 to 4 % respectively and to obtain a regular stacking of the layers.

To complete these tests and to understand the impact of the formulation such as aluminosilicate source (M1, M2, A650), reinforcement elements (W, G), and fillers (A, Ki, Sa), on the slump rate, different composition were elaborated by 3D printing. The different compositions and reported in **Table 2** and the slump rate is plotted as a function of the liquid to solid ratio (L/S) in **Figure 3.** Whatever the formulation, the slump rate values decrease with the L/S ratio. This can be explained by the addition of reinforcements and fillers and/or the modification of polycondensation reactions [x]. Firstly, the geopolymer binder without additives (M_{16}) presents a slump rate of 100 % as the viscosity (or/and yield stress) of the binder is not enough to realize additive manufacturing. By modifying the viscosity, the addition of glass fibers ($M_{16}G_4$) leads to a decrease in the slump rate value of 77 %. In the same way, the addition of wollastonite ($M_{16}W_{21}$) permits to reach of a slump rate of 23 %. A larger amount of wollastonite is not possible, the mixture becoming too grainy. These results are in agreement

with previous works [xiii, xiv] where the addition of wollastonite and glass fibers increases the viscosity of the binder. The modification of reaction kinetics by the wollastonite and the steric hindrance of the glass fibers improve the stabilization of the layers under the impact of gravity and reduce the slump of the printed material. The combination of wollastonite and glass fibers ($M_{16}W_{10}G_4$, $M_{16}W_{21}G_2$) validates these results and permits them to obtain a minimum rate slump of 16 and 19 % respectively. Moreover, the increasing of the metakaolin content ($M_{19}W_{10}G_2$) decreases the slump rate at 9 % due to promoted polycondensation reactions and the augmentation of the solid fraction and viscosity [xlvi].

The viscosity of the formulation can also be modified with reactive or non-reactive aluminosilicate sources [xlvii]. In the case of the modification of the reactive aluminosilicate source with the addition of more reactive metakaolin (M2) [xlii] and calcined argillite ($M^*W_{21}G_2$), the slump rate does not decrease (17 %). The modification of the reactivity of the mixture is not enough to decrease the slump rate. In the case of the addition of non-reactive aluminosilicates such as raw argillite (A) and kaolin (Ki) the slump rate decreases to 8, 4, and 2 % for the $M_{16}W_{21}G_2A_6$, $M_{16}W_{10}G_2A_{10}$, and $M_{16}W_{10}G_2A_{10}Ki_2$ compositions, respectively. The addition of sand ($M_{16}W_{21}G_2Sa_6$) induces also a decrease of the slump rate (8%). The pulverulent fillers allow stabilizing the layers without reaching the granular or fibrous appearance obtained with an excess of wollastonite or glass fibers. From these data, it is found that, by increasing their amount, the layers are more stable and the buildability of the material is increased. To succeed in the printing, the slump rate can be decreased either by the modification of the polycondensation reaction (aluminosilicate source amount), or by the addition of wollastonite that modifies the polycondensation reaction, or by the addition non-reactive fillers such as glass fibers or argillite that decreases the L/S ratio.

3.2 Printing speed, adhesion of layers and storage conditions (T, % RH)

To optimize the slump rate, the printing speed (v_z) has also been studied by modifying the nozzle speed (v_n). The photos and slump values of the formulation $M_{14}W_{21}G_2A_6Sa_{10}$ shaped with different printing speed are reported in **Table 2**. The slump rate decreases with the printing speed. A vertical printing speed of 248.10^{-6} m/s gives a slump rate of 20 % with an irregular stacking of the layers. By dividing this printing speed by two and by four, the slump rate becomes respectively 14 % and 3 % and the layers are more evenly stacked. A slower printing speed induces indeed a longer time between two layers and the polycondensation reactions are promoted before the deposition of a new layer. The printing speed must be adapted to the composition used (setting time) and to the piece to be produced (dimensions, printing path).

Different printing speed (v_z) implies different times between layers. To verify the adhesion between the layers as a function of time, two layers of a composition M_{19} have been extruded with a syringe (Φ_{nozzle} = 2 mm) with different time intervals (1 and 240 minutes). The SEM photos of the freshly extruded geopolymer (**Figure 4)** show different interfaces between the layers depending on the time interval. For a short time interval, (**Figure 4-a**), the interface between the layers is almost imperceptible and conduce to a mix of the material inducing a strong adhesion of the layers. Conversely, for a long time interval (**Figure 4-b)**, an interface between the layers of a few tens of micrometers is visible. In the latter case, the polycondensation reactions have started, which induces the formation of an interface and limiting interaction with the second layer. Therefore, the time between two layers should not be too long for the layers to adhere to each other. For each formulation, an adequate speed between a too high speed causing the collapse of the layers and a too low speed reducing the adhesion of the layers must be optimized. Other parameters to take into account are the relative humidity and the temperature. To evaluate their impact, the evolution of the consolidation ($M_{16}W_{15}$) of two extruded layers (Φ_{nozzle} = 2 mm) with a time interval of 1 minute has been

observed with an ESEM and a Peltier module **Table 4**. To obtain a pressure of 1000 Pa allowing observation, three conditions of temperature and relative humidity were selected (43 % RH / 20 °C, 63 % RH / 14 °C, 93 % RH, 8°C). The extruded reactive mixture shows different changes over time depending on the environmental conditions. For the 20 °C / 43 % RH condition, at t = 15 min, the interface between the layers is imperceptible. From t = 25 min, the microstructure typical of a geopolymer is notable, as well as wollastonite needles. This phenomenon is linked to the consolidation of the material over time. The 14 °C / 63 % RH condition induces the same phenomena with a little slower setting. A lower temperature and a lower relative humidity (8 °C / 93 % RH) do not make the consolidation possible. An acquisition at 100 minutes revealed that the material had completely collapsed. Thus, it is possible to obtain pieces with a range of temperatures from 14 to 20°C coupled with a range of relative humidity from 43 to 63 % RH. The use of different reinforcements or inorganic fillers as well as the adaptation of the printing speed allows to shape geopolymer composite by additive manufacturing with a limited slump and a defined range of temperature and relative humidity.

3.3 Mechanical properties of shaping pieces

To analyze the impact of shaping on mechanical properties, bending specimens were shaped by casting and 3D printing with the formulation $M_{16}W_{10}G_2$. The specimens were tested in three-point bending in two directions of solicitation (**see Figure 1**). The photos after rupture as well as the stress curves as a function of the strains are presented in **Figure 5**. The samples have similar failure profiles and maximum stresses. The photos of the specimens after failure (**Figure 5-A)** show that the casted sample has no defect. On the contrary, the printed samples have some voids due to the shaping process. These voids have also been observed in the literature [xxxvi, xli] with printed alkali-activated material. Moreover, the fact that the cracking caused by the rupture does not follow the interface between the layers, underlines a strong adhesion between the layers [xxxv].

The stress curves as a function of the deformation (**Figure 5-B)** exhibit the same behavior: an elastic regime is first observed followed by a more or less ductile rupture. The samples produced by casting have maximum bending stress of 15 $\pm$ 2 MPa. The samples produced by 3D printing show identical values regardless of the directions of solicitation, which is in agreement with the hypothesis of strong adhesion between the layers. The presence of voids should cause a reduction in the bending stress, however, this can be compensated by the orientation of the fibers perpendicular to the direction of stress [xxxii]. To verify the orientation of fibers during extrusion, the microstructure sample $M_{16}W_{10}G_2$ shaped by 3D printing was observed (**Figure 6)**. The microstructure of the printed sample shows an orientation of the fibers along the printing direction and confirms the previous results.

3.4 Comparison with literature data

To compare the mechanical properties obtained in this study with those of the literature, the flexural stress values of binders and short fibers concrete and alkali-activated composites elaborated by additive manufacturing, are gathered in **Figure 7.** To our knowledge, there is no mechanical test in the literature on printed geopolymer composites made with metakaolin and without organic additives. Wolf et al. [xlviii] tested concrete printed specimens elaborated with different interlayer interval times, nozzle height, or surface hydration, and found flexural stress values from 3 to 4 MPa. Bos et al. [xlix] studied the addition of fibers and showed that the fibers cause an important increase in the flexural strength of the printed samples (from 1 to 6 MPa) due to the orientation of fibers. Le et al. [xxxviii] used a high-performance concrete with polypropylene fibers and increases the flexural strength from 11 MPa for the casted samples to 12 and 13 MPa for the printed depending on the direction of solicitation of the stacked layers. For the printed alkali-activated materials based on fly ash, Panda et al. [xxxi] added 0,25 % to 1 % of 3 to 8 mm glass fibers and exhibit flexural strength from 5 to 7 MPa. Some authors obtained similar values depending on the tested direction (6 to 7 MPa) [xxvi] or the time interval

(3 to 5 MPa) [xxxvii]. Higher flexural strengths were observed for the printed material in comparison to the control casted samples (from 8 to 10 MPa and from 6 to 7 MPa respectively for Korniejenko et al. [l] and Paul et al. [xxvii]. For the same material composition, the variation on the flexural strength is mainly dependent on the printing speed and the testing direction (linked with fibers orientation). The variation of flexural strength values found in the literature seems to come from the type of material used. A high-performance material will also present a high (or even better) performance by additive manufacturing. The mechanical strengths obtained in this study (15 MPa with $M_{16}W_{10}G_2$) can be explained by the maintenance of the mechanical properties of the geopolymer between the casted and printed material. These results are characteristic of an adapted printing speed, a good adhesion between the layers, and the orientation of the fibers that counterbalance the negative effect due to the presence of voids. Moreover, this study exhibits higher flexural strength values than those found in the literature.

The mechanical properties of the geopolymer composite filling the specifications, it will be tested and shaped in future work on a larger scale with a 6 axis-robot and an adapted own-developed extruding tool to elaborate the prototype of cell liner (**Figure 8**).

4. CONCLUSION

This study focuses on geopolymer composites shaping by additive manufacturing without organic compounds. To obtain an adequate formulation, inorganic reinforcement and filler elements were added and the geopolymerization reactions were evaluated with shrinkage measurement. The process was adapted and the adhesion of layers was controlled with different time intervals and storage conditions. The flexural strength of the printing material was measured and compared with the flexural strength of printed materials in the literature. It has been shown that:

- the geopolymer composite formulation could be shaped by 3D printing and the slump rate could be decreased by adding metakaolin, wollastonite, glass fibers or non-reactive aluminosilicate, without the use of organic compounds;
- the decreasing of the printing speed and the use of the inorganic elements reduce the slump observed during the printing;
- the layers exhibit a good adhesion between them with conditions of time, temperature and relative humidity (14 – 20 °C and 43 – 63 % RH) and the fibers are oriented parallel to the printing path during the process;
- A flexural strength of 15 MPa was obtained for the printed material.

The use of additive manufacturing to shape geopolymer composite with inorganic reinforcement and fillers seems therefore to be promising and will be tested at a larger scale in future work.

Acknowledgments

We thank the French National Radioactive Waste Management Agency (Andra) for the funding of this research.

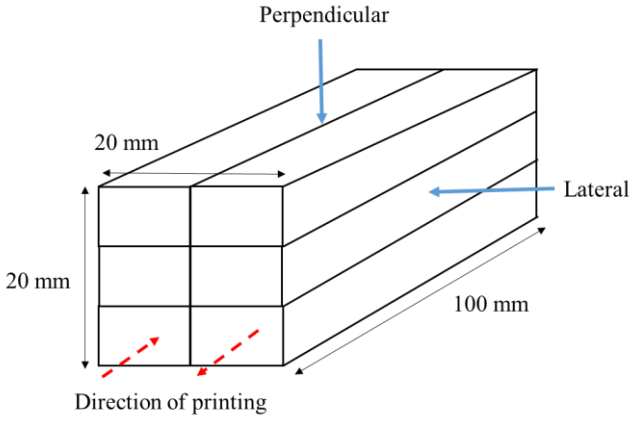

Figure 1: schema of the 3-point bending specimen obtained by robocasting and tested directions of solicitation.

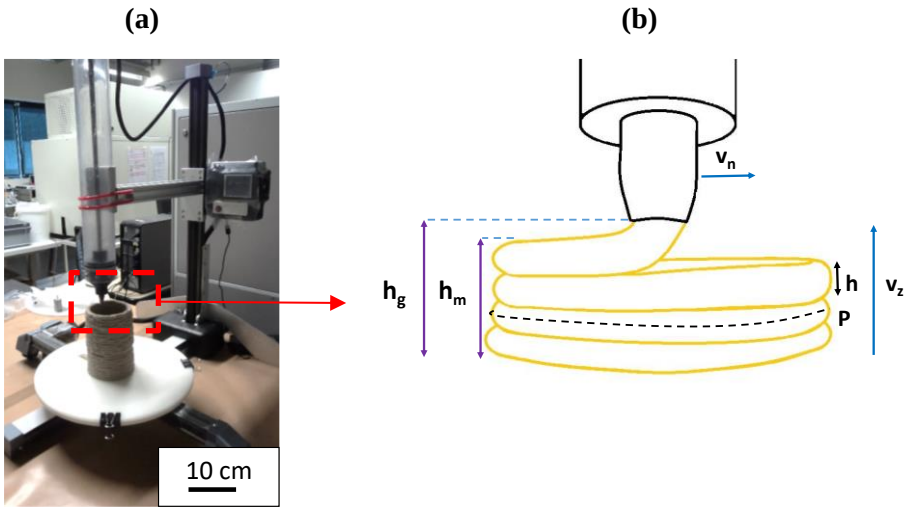

Figure 2: (a) the 3D printer (3D Potterbot) and **(b)** the printing parameters.

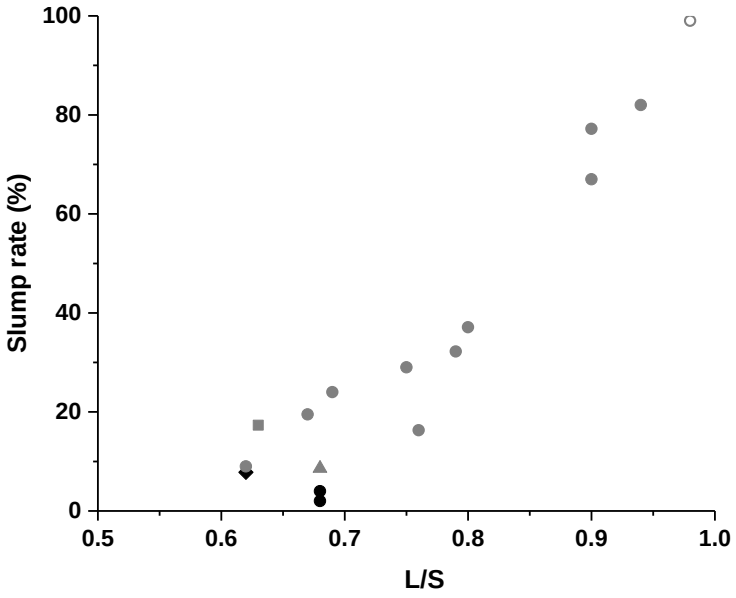

Figure 3: slump rate as function of the ratio L/S for the formulations shaped with the robocasting process (v_z = 62.10^{-6} m/s) with (○) the M_{16} binder and the (●) $M_{16}W_aG_b$, (▲) $M_{19}W_{10}G_2$, (■) $M^*W_{21}G_2$, (●) $M_{16}W_aG_bA_cKi_d$ and (◆) $M_{16}W_{21}G_2Sa_6$ composites (see Table 2).

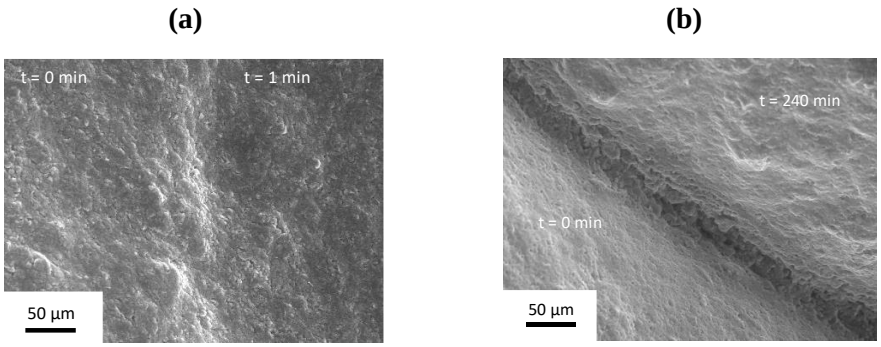

Figure 4: SEM photos of the interface between two fresh layers of a geopolymer M_{19} extruded with a syringe (Φ_{buse} = 2 mm) with a time gap of **(a)** 1 and **(b)** 240 minutes.

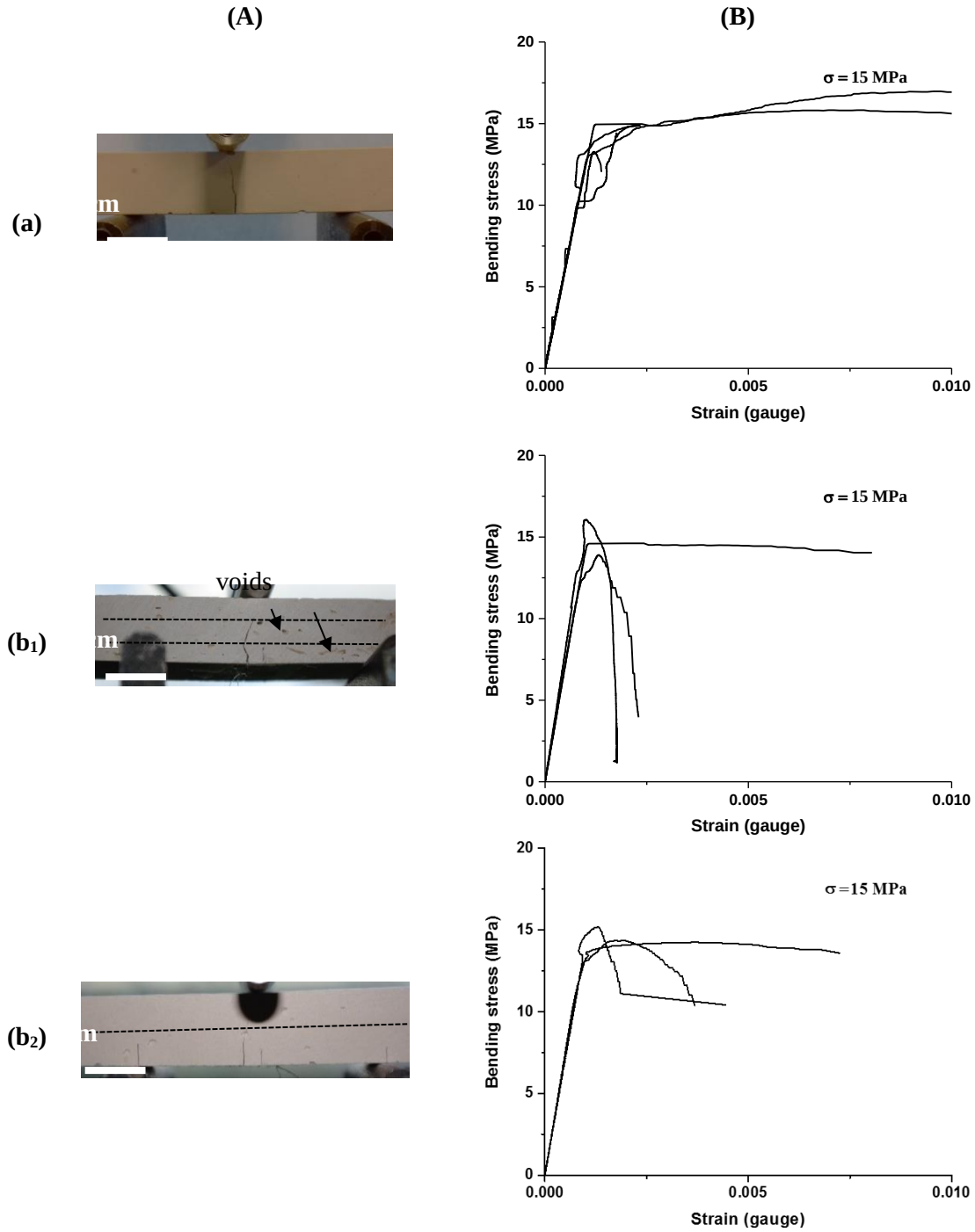

Figure 5: (A) photos after failure and **(B)** axial stress as a function of strain for the 3-points bending samples elaborated by **(a)** casting and by robocasting in **(b_1)** perpendicular and **(b_2)** lateral directions (see Figure 1).

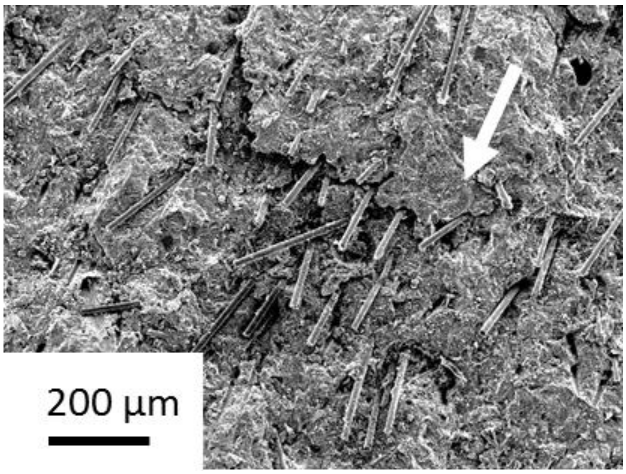

Figure 6: SEM photos of the microstructure of $M_{16}W_{10}G_2$ geopolymers shaped by robocasting (↗ represent the printing direction).

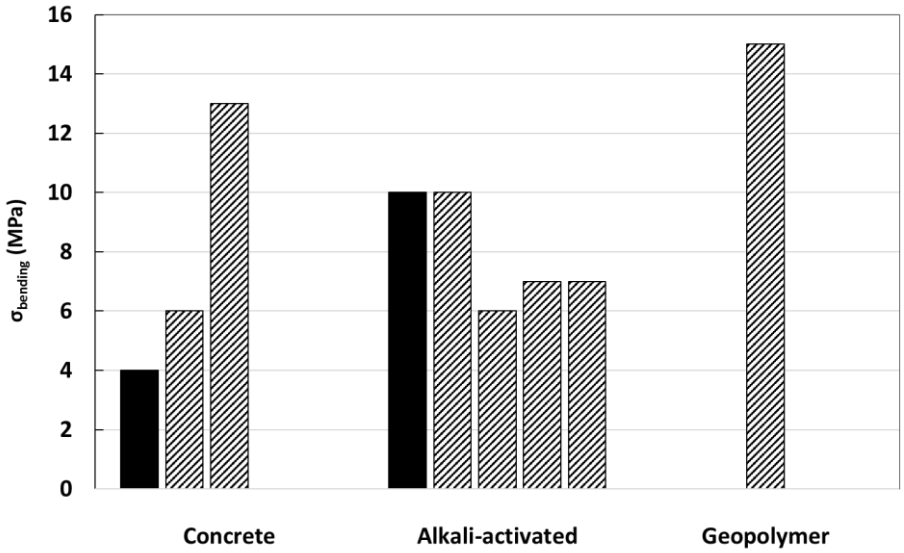

Figure 7: bending values in the literature for concretes (Wolf et al. 2019, Bos et al. 2019, Le et al. 2012), alkali-activated materials (Paul et al. 2018, Bong et al 2019, Al-Qutaifi et al 2018, Panda et al. 2017, Korniejenko et al. 2019) and geopolymers (values from this study) for ■ binders and ▨ composites shaped by robocasting.

Figure 8: a geopolymer own-developed extruding tool mounted on a 6-axis robot (Build'In platform).

Table 1: Physico-chemical data on the alkaline solution, metakaolin, and fillers.

		Name	Supplier	Composition (%w)	Furnace	Size (µm)
Solution	**Potassium silicate**	S3	Woellner	SiO_2: 19.0 K_2O: 22 .0 H_2O: 59.0		
Alumino-silicate sources	**Metakaolins**	M1	Imerys	SiO_2: 55.0 Al_2O_3: 40.0	Rotary	D_{50} = 10
		M2		SiO_2: 55.0 Al_2O_3: 39.0	Flash	D_{50} = 8
	Calcined argillite	A650	Andra	SiO_2: 49.0 Al_2O_3: 13.0	Static	D_{50} = 28
Reinforcement elements	**AR glass fibers**	G	Owens Corning	SiO_2: 55.0 K_2O: 20.0 ZrO_2: 20.0		L = 6000 Φ = 13 -15
	Wollastonite	W	Imerys	SiO_2: 55.0 CaO: 45.0		L = 5-170 Φ = 3-15
Powdered fillers	**Argilite**	A	Andra	SiO_2: 49.0 CaO : 11.0 Al_2O_3: 13.0 MgO : 3.0 Fe_2O_3: 5.0 K_2O: 2.0		D_{50} = 17
	Kaolin BIP	Ki	Kaolin de Beauvoir	SiO_2 : 48.0 Al_2O_3 : 39.0 K_2O : 2.0		20 2
	Sand S8	Sa	Sibelco	SiO_2 : 99.8		D_{50} = 250

Table 2: compositions elaborated by robocasting (Φ = 10 mm, $v_z = 62.10^{-6}$ m/s), liquid sur solid *ratio* and slump rate measured (M= metakaolin M1, M*= $M1_{12}M2_{1.4}A650_{3.2}$, W = wollastonite, G = glass fiber, A = raw argillite, Ki = kaolin, Sa = sand).

Composition	L/S	Slump rate (%)	code
$\mathbf{M_{16}}$	0.98	100	○
$\mathbf{M_{16}W_{15}}$	0.75	29	●
$\mathbf{M_{16}W_{21}}$	0.69	23	●
$\mathbf{M_{16}G_2}$	0.94	82	●
$\mathbf{M_{16}G_4}$	0.90	77	●
$\mathbf{M_{16}W_{10}G_1}$	0.80	37	●
$\mathbf{M_{16}W_2G_2}$	0.90	67	●
$\mathbf{M_{16}W_{10}G_2}$	0.79	32	●
$\mathbf{M_{16}W_{10}G_4}$	0.76	16	●
$\mathbf{M_{16}W_{21}G_2}$	0.67	19	●
$\mathbf{M_{19}W_{10}G_2}$	0.68	9	▲
$\mathbf{M^*W_{21}G_2}$	0.63	3	■
$\mathbf{M_{16}W_{10}G_2A_{10}}$	0.68	4	●
$\mathbf{M_{16}W_{10}G_2A_{10}Ki_2}$	0.66	2	●
$\mathbf{M_{16}W_{21}G_2A_6}$	0.62	8	●
$\mathbf{M_{16}W_{21}G_2Sa_6}$	0.62	9	◆

Table 3: values of printing speed (v_z), of slump rate, and corresponding photos for different compositions elaborated by robocasting.

Composition	vz ($.10^{-6}$ m/s)	Slump rate (%)	Photo design
$M_{16}W_2G_2$	62	67	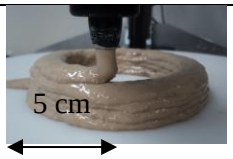
$M_{16}W_{10}G_2$		32	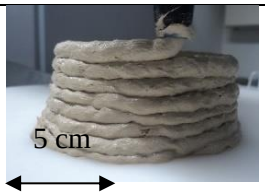
$M_{16}W_{10}G_2A_{10}$		4	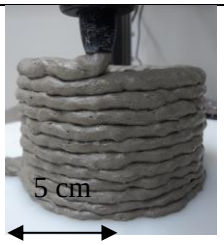
$M_{14}W_{21}G_2A_6Sa_{10}$	62	3	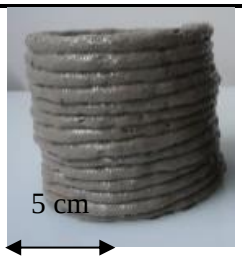
	124	14	
	248	20	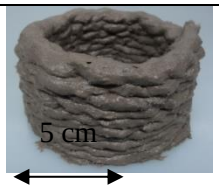

Table 4: ESEM photos of the evolution in time for a composite $M_{16}W_{15}$ extruded with a syringe (Φ_{buse} = 2 mm) in three conditions of temperature and relative humidity.

T (°C) / RH (%)	Time (min)		
	15	**35**	**55**
20 / 43	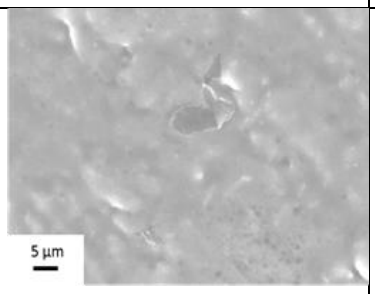	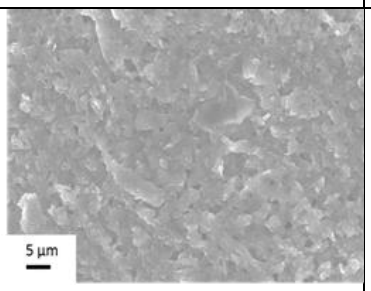	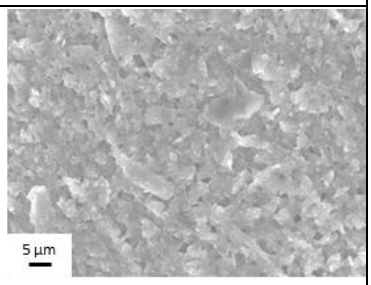
14 / 63	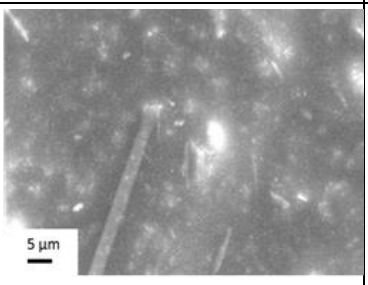	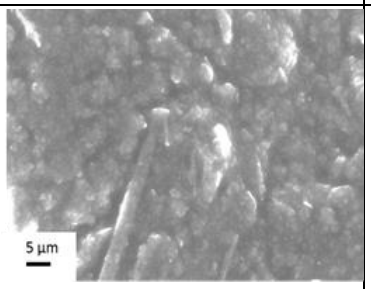	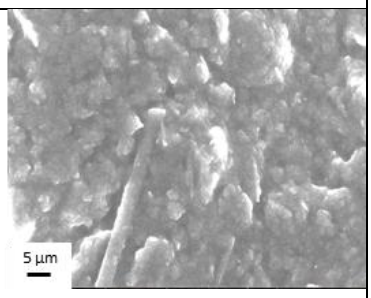
8 / 93	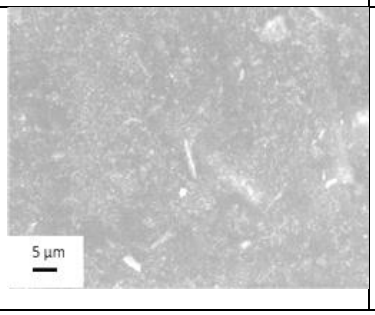	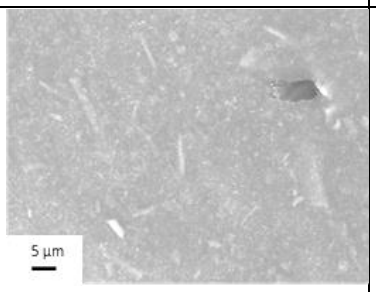	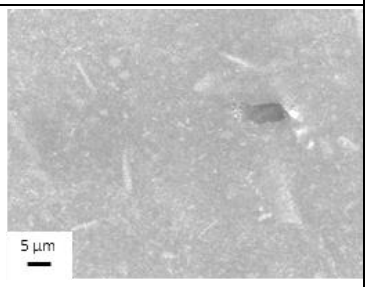

5. REFERENCES

[i] Davidovits J., 2008. Geopolymer Chemistry and Applications, 2nd ed. Saint-Quentin, France: Institut Geopolymer.

[ii] Davidovits J., 2018. Why Alkali-Activated Materials (AAM) are Not Geopolymers, Technical Paper #25, Geopolymer Institute Library. 10.13140/RG.2.2.34337.25441

[iii] Skvara F., 2007. Alkali active materials or geopolymers? Ceramics. 51, 173-177.

[iv] Provis, J. L., van Deventer, J. S. J., 2019. Geopolymers and Other Alkali-Activated Materials. Lea's Chemistry of Cement and Concrete. 779–805.10.1016/b978-0-08-100773-0.00016-2

[v] Zhao Q., Nair B., Rahimian T., Balaguru P., Novel P., 2007. Geopolymer based composites with enhanced ductility. Journal of Materials Science. 42, 3131-3137. 10.1007/s10853-006-0527-4.

[vi] Li Z., Zhang Y., Zhou X, 2005. Short fiber reinforced geopolymer composites manufactured by extrusion. Journal of Materials in Civil Engineering. 17, 624-631. 10.1061/(ASCE)0899-1561(2005)17:6(624).

[vii] Sé Ribeiro R.A., Sà Ribeiro M.G., Kriven W.M., 2017. A review of particle and fiber-reinforced metakaolin based geopolymer composites. J. Ceram. Sci. Technol. 8, 302-322. 10.4416/JCST2017-00048.

[viii] Steinerova M., Matulova L., Vermach P., Kotas J., 2017. The Brittleness and chemical stability of optimized geopolymer composites. Materials. 10, 396-416. 10.3390/ma10040396.

[ix] Nurjaya D., Astutiningsih S., Zulfia A., 2015. Thermal effect on flexural strength of geopolymer matrix composite with alumina and wollastonite as fillers. International journal of technology. 03, 462-470. 10.14716/ijtech.v6i3.1441.

[x] Archez J., Texier-Mandoki N., Bourbon X., Caron J.F., Rossignol S., 2020. Influence of the aluminum concentration, wollastonite and glass fibers on geopolymer composites workability and mechanical properties. Construction and Building Materials. 119511. 10.1016/j.conbuildmat.2020.119511.

[xi] Peyne J., Joussein E., Gautron J., Doudeau J., Rossignol S., 2017. Feasibility of producing geopolymer binder based on a brick clay mixture. Ceramics International. 43, 9860-9871. 10.1016/j.ceramint.2017.04.169.

[xii] Chindaprasirt P., Chareerat T., Sirivivatnanon V., 2007. Workability and strength of coarse high calcium fly ash geopolymer. Cement and concrete composites. 29, 224-229. 10.1016/j.cemconcomp.2006.11.002.

[xiii] Soliman A.M., Nehdi M.L., 2012. Effect of Natural Wollastonite Microfibers on Early-Age Behavior of UHPC. Journal of Materials in Civil Engineering. 24, 816-824. 10.1061/(ASCE)MT.1943-5533.0000473.

[xiv] Alomayri T., 2017. The microstructural and mechanical properties of geopolymer composites containing glass microfibers. Ceramics International. 43, 4576-4582. 10.1016/j.ceramint.2016.12.118.

[xv] Cesarano J. A, 1999. Review of Robocasting Technology. Mater Res Soc Symp Proc. 542, 133-139. 10.1557/PROC-542-133.

[xvi] Buswell R.A., Leal de Silva W.R., Jones S.Z., Dirrenberger J., 2018. 3D printing using concrete extrusion: a roadmap for research. Cement and concrete research.112, 37-49. 10.1016/j.cemconres.2018.05.006.

[xvii] Franchin G., Scanferla P., Zeffiro L., Elsayed H., Baliello A., Giacomello G., Pasetto M., Colombo P., 2017. Direct ink writing of geopolymeric inks. Journal of the European Ceramic Society. 37, 2481-2489. 10.1016/j.jeurceramsoc.2017.01.030.

[xviii] Agnoli E., Ciapponi R., Levi M., Turri S., 2019. Additive Manufacturing of Geopolymers Modified with Microalgal Biomass Biofiller from Wastewater Treatment Plants. Materials. 12, 1004. 10.3390/ma12071004.
[xix] Hambach M., Volkmer D., 2017. Properties of 3D-printed fiber-reinforced Portland cement paste. Cement and Concrete Composites. 79, 62-70. 10.1016/j.cemconcomp.2017.02.001.
[xx] Nerella V. N., Mechtcherine V., 2019. Studying the Printability of Fresh Concrete for Formwork-Free Concrete Onsite 3D Printing Technology (CONPrint3D). 3D Concrete Printing Technology. chapter 16, 333-347. 10.1016/B978-0-12-815481-6.00016-6.
[xxi] Bos F., Wolfs R., Ahmed Z., Salet T., 2016. Additive manufacturing of concrete in construction: potentials and challenges of 3D concrete printing. Virtual and physical prototyping. 11, 209-225. 10.1080/17452759.2016.1209867.
[xxii] Zhang Y., Zhang Y., Liu G., Yang Y., Wu M., Pang B., 2018. Fresh properties of a novel 3D printing concrete ink. Construction and Building Materials. 174, 263-271, 2018. 10.1016/j.conbuildmat.2018.04.115.
[xxiii] Panda B., Unluer C., Tan M.J., 2018. Investigation of the rheology and strength of geopolymer mixtures for extrusion-based 3D printing. Cement and concrete composite. 94, 307-314. 10.1016/j.cemconcomp.2018.10.002.
[xxiv] B. Panda, C. Unluer, M.J. Tan, 2019. Extrusion and rheology characterization of geopolymer nanocomposites used in 3D printing. Composites part B. 176, 107290. 10.1016/j.compositesb.2019.107290.
[xxv] B. Panda, S. Ruan, C. Unluer, M.J. Tan, 2020. Investigation of the properties of alkali-activated slag mixes involving the use of nanoclay and nucleation seeds for 3D printing. Composites Part B: Engineering. vol. 186, 107826. 10.1016/j.compositesb.2020.107826.
[xxvi] Bong S.H., Nematollahi B., Nazari A., Xia M., Sanjayan J.G., 2019. Fresh and Hardened Properties of 3D Printable Geopolymer Cured in Ambient Temperature. 1st RILEM Bookseries. 19, 3-11. 10.1007/978-3-319-99519-9_1.
[xxvii] Paul S. C., Tay Y.W.D., Panda B., Tan M.J., 2018. Fresh and hardened properties of 3D printable cementitious materials for building and construction. Civil and Mechanical Engineering. 18, 311-319. 10.1016/j.acme.2017.02.008.
[xxviii] Panda B., Paul S.C, Hui J.L., Tay Y.W.D., Tan M.J., 2017. Additive manufacturing of geopolymer for sustainable built environment. Journal of Cleaner Production. 167, 281-288. 10.1016/j.jclepro.2017.08.165.
[xxix] Regulation (EC) No 1907/2006 of the European Parliament and of the council of 18 December 2006, Official Journal of the European Union, L136/3, 2007.
[xxx] Nematollahi B., Xia M., Bong S.H., Sanjayan J., 2019. Hardened Properties of 3D Printable 'One-Part' Geopolymer for Construction Applications. RILEM Bookseries. 19, 190-199. 10.1007/978-3-319-99519-9_17.
[xxxi] Panda B., Paul S.C., Tan M. J., 2017. Anisotropic mechanical performance of 3D printed fiber-reinforced sustainable construction material. Materials letters. 209, 146-149. 10.1016/j.matlet.2017.07.123.
[xxxii] Shimamoto D., Tominaga Y., Imai Y., Hotta Y., 2016. Fiber orientation and flexural properties of short fiber/epoxy composites. Journal of the Ceramic Society of Japan. 124, 125-128. 10.2109/jcersj2.15120.
[xxxiii] Nerella V. N., Hempel S., Mechtcherine V., 2019. Effects of layer-interface properties on mechanical performance of concrete elements produced by extrusion-based 3D-printing. Construction and Building Materials. 205, 586-601. 10.1016/j.conbuildmat.2019.01.235.
[xxxiv] Wangler T., Lloret E., Reiter L., Hack N., Gramazio F., Kohler M., Bernhard M., Dillenburger B., Buchli J., Roussel N., Flatt R., 2016. Digital Concrete: Opportunities and Challenges. RILEM Technical Letters. 10, 67-75. 10.21809/rilemtechlett.2016.16.

[xxxv] Sanjayan J.G., Nematollahi B., Xia M., Marchment T., 2018. Effect of surface moisture on inter-layer strength of 3D printed concrete. Construction and building materials. 172, 468-475. 10.1016/j.conbuildmat.2018.03.232.
[xxxvi] Panda B., Paul S. C, Mohamed N.A.N, Tay Y.W.D., Tan M.J., 2018. Measurement of tensile bond strength of 3D printed geopolymer mortar. Measurement. 103, 108-116. 10.1016/j.measurement.2017.08.051.
[xxxvii] Al-Qutaifi S., Nazari A., Bagheri A., 2018. Mechanical properties of layered geopolymer structures applicable in concrete 3D-printing. Construction and building materials. 176, 690-699. 10.1016/j.conbuildmat.2018.04.195.
[xxxviii] Le T.T., Austin A., Lim S., Buswell R.A., Law R., Gibb A.G.F., Thorpe T., 2012. Hardened properties of high-performance printing concrete. Cement and Concrete Research. 42, 558-566. 10.1016/j.cemconres.2011.12.003.
[xxxix] Lao W., Tay D.Y.W., Quirin D., Tan M. J., 2018. The effect of nozzle shapes on the compactness and strength of structures printed by additive manufacturing of concrete. Proceedings of the 3rd International Conference on Progress in Additive Manufacturing. 80-86. 10.25341/D4V01X
[xl] Nematollahi B., Vijay P., Sanjayan J., Nazari A., Xia M., Nerella V.N., Mechtcherine V., 2018. Effect of polypropylene fibre addition on properties of geopolymers made by 3D printing for digital construction. Materials. 11, 2352-2368. 10.3390/ma11122352.
[xli] Nematollahi B., Xia M., Sanjayan J., Vijay P, 2018. Effect of type of fiber on inter-layer bond and flexural strengths of extrusion-based 3D printed geopolymer. Material Science Forum. 939, 155-162. 10.4028/www.scientific.net/MSF.939.155.
[xlii] Autef A., 2013. Formulation géopolymère : influence des rapports molaires Si/K et Si/Al sur les réactions de polycondensation au sein des gels aluminosilicatés. Doctoral thesis. University of Limoges.
[xliii] Dupuy C., Gharzouni A., Texier-Mandoki N., Bourbon X., Rossignol S., 2018. Thermal resistance of argillite-based alkali-activated materials. Part I: effect of calcination processes and alkali cation. Materials Chemistry and Physics. 217, 323-333. 10.1016/j.matchemphys.2018.06.079.
[xliv] A. Gharzouni, E. Joussein, B. Samet, S. Baklouti, S. Rossignol, 2015. Effect of the reactivity of alkaline solution and metakaolin on geopolymer formation. Journal of Non-crystalline Solids. 410, 127-134. https://doi.org/10.1016/j.jnoncrysol.2014.12.021
[xlv]Archez J., Texier-Mandoki N., Bourbon X., Caron J.F. and Rossignol S., 2020. Adaptation of the geopolymer composite formulation to the shaping process. Materials Today Communication, 25, 101501. 10.1016/j.mtcomm.2020.101501.
[xlvi] Romagnoli M., Leonelli C., Kamseu E., Gualtieri M.L., 2012. Rheology of geopolymer by DOE approach. *C*onstruction and Building Materials. 36, 251-258. 10.1016/j.conbuildmat.2012.04.122.
[xlvii] Arnoult M., Perronnet M., Autef A., Rossignol S., 2019. Geopolymer synthesized using reactive or unreactive aluminosilicate. Understanding of reactive mixture. Materials Chemistry and Physics. 237, 121837. 10.1016/j.matchemphys.2019.121837.
[xlviii] Wolfs R.J.M., Bos F.P., Salet T.A.M, 2019. Hardened properties of 3D printed concrete: the influence of process parameters on interlayer adhesion. Cement and Concrete Research. 119, 132-140. 10.1016/j.cemconres.2019.02.017.
[xlix] Bos F. P., Bosco E., Salet T. A. M., 2019. Ductility of 3D printed concrete reinforced with short straight steel fibers. Virtual and Physical Prototyping. 14, 160-174. 10.1080/17452759.2018.1548069.
[l] Korniejenko K., Lach M., Chou S.Y., Lin W.T., Mikula J., Mierzwinski D., Cheng A., Hebda M., 2019. A comparative study of mechanical properties of fly ash-based geopolymer made by

casted and 3D printing method. Materials Science and Engineering. 660, 012005. 10.1088/1757-899X/660/1/012005.